IEICE Electronics Express, Vol.19, No.18, 1–5

LETTER

Behavior of intercore crosstalk in square-layout uncoupled four-core fibers

Masanori Koshiba[1, a)], **Yasuo Kokubun**[2], **Mayu Nakagawa**[3], **Masaki Ohzeki**[3], **and Katsuhiro Takenaga**[3]

Abstract Recently, a very interesting behavior of crosstalk (XT) between diagonal cores (diagonal XT) in a square-layout uncoupled four-core fiber (UC-4CF) that grows quadratically with fiber length has been reported. In this paper, the behavior of intercore XT in square-layout UC-4CFs is investigated on the basis of a coupled-power theory. To make it easy to understand the physical mechanism of intercore XT behavior, we derive an approximate solution of coupled-power equations. We show that there exists a range of fiber lengths within which the diagonal XT grows quadratically. Finally, we propose a heterogeneous square-layout UC-4CF in which intercore XT could be further suppressed.

Keywords: four-core fiber, intercore crosstalk, coupled-power theory
Classification: Optical hardware (fiber optics, microwave photonics, optical interconnects, photonic signal processing, photonic integration and modules, optical sensing, etc.)

1. Introduction

Uncoupled multicore fibers (MCFs) with the standard 125-μm cladding have attracted attention because conventional cabling and splicing technologies can be effectively adopted for such fibers: two-core fibers [1], four-core fibers [2, 3, 4, 5, 6], five-core fibers [7, 8], and eight-core fibers [9, 10]. Recently, high-capacity and/or long-haul transmission experiments have been successfully performed using a square-layout uncoupled four-core fiber (UC-4CF) with a standard cladding diameter [11, 12, 13, 14]. The square-layout UC-4CF is also suitable for bidirectional transmissions [15] in which intercore crosstalk (XT) is suppressed by assigning opposite signal propagation directions between adjacent cores [16, 17, 18, 19]. XT in bidirectional transmissions is predominantly induced by Rayleigh backscattered XT (XT_{bs}) and back-reflected XT (XT_{refl}) from counterpropagating signals in the nearest neighboring cores, as well as diagonal XT (XT_{diag}), i.e., XT between diagonal cores [15]. In bidirectional transmissions with square-layout UC-4CFs, care should be taken for not only XT_{bs} and XT_{refl} but also XT_{diag} because signals in diagonal cores are transmitted in the same direction.

In general, adjacent XT (XT_{adj}), i.e., intercore XT between adjacent cores, grows linearly with fiber length [20, 21, 22, 23]. More recently, Nakagawa *et al.* [24] have measured intercore XT in a square-layout UC-4CF and found a very interesting behavior of XT_{diag} that grows quadratically with fiber length.

In this paper, the behavior of intercore XT in square-layout UC-4CFs is investigated on the basis of a coupled-power theory [20, 21, 22, 23]. To make it easy to understand the physical mechanism of intercore XT behavior, we derive an approximate solution of coupled-power equations and confirm that XT_{diag} is induced by direct XT (XT_{dir}) from a diagonal core and indirect XT (XT_{indir}) via adjacent cores. XT_{dir} and XT_{indir} grow linearly and quadratically with fiber length, respectively. We show that XT_{diag} has a specific fiber length at which XT_{dir} and XT_{indir} are equal to each other. This length gives us a lower bound of fiber length beyond which XT_{indir} becomes predominant, $XT_{diag} \approx XT_{indir}$. We also show that there is an upper bound of fiber length below which XT_{diag} grows quadratically. As a result, we conclude that whether XT_{diag} grows linearly or quadratically depends on fiber length. Finally, to further suppress not only XT_{diag} but also XT_{bs} and XT_{refl}, we propose a square-layout UC-4CF with heterogeneous cores.

2. Solutions of coupled-power equations

We consider the square-layout UC-4CF with homogeneous cores shown in Fig. 1(a). Fig. 1(b) shows a cross section of the fabricated step-index profile UC-4CF with the standard 125-μm cladding [24].

Assuming that all cores are homogeneous (identical), coupled-power equations are given by [24, 25]

$$\frac{dP_1(z)}{dz} = h(P_2 - P_1) + g(P_3 - P_1) + h(P_4 - P_1), \quad (1a)$$

$$\frac{dP_2(z)}{dz} = h(P_1 - P_2) + h(P_3 - P_2) + g(P_4 - P_2), \quad (1b)$$

$$\frac{dP_3(z)}{dz} = g(P_1 - P_3) + h(P_2 - P_3) + h(P_4 - P_3), \quad (1c)$$

$$\frac{dP_4(z)}{dz} = h(P_1 - P_4) + g(P_2 - P_4) + h(P_3 - P_4), \quad (1d)$$

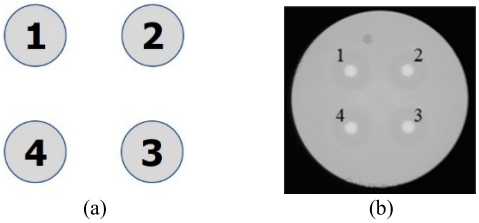

(a) (b)

Fig. 1 (a) Schematic and (b) cross section [24] of a square-layout UC-4CF with homogenous cores.

[1] Hokkaido University, Sapporo 060-0814, Japan
[2] Institute of Technologists, 333 Maeya, Gyoda 361-0038, Japan
[3] Optical Technologies R&D Center, Fujikura Ltd., 1440 Mutsuzaki, Sakura 285-8550, Japan
[a)] koshiba@wave.plala.or.jp

DOI: 10.1587/elex.19.20220379
Received August 21, 2022
Accepted August 23, 2022
Publicized August 31, 2022
Copyedited September 25, 2022

Table I Analytical expressions for intercore crosstalk in square-layout UC-4CFs with homogeneous cores: exact crosstalk [24, 25] and approximate crosstalk (this work).

g	XT	Exact XT	Approx. XT
$g \neq 0$	$\mathrm{XT}_{\mathrm{adj}}$	$\dfrac{1-\mathrm{e}^{-4hL}}{1+2\mathrm{e}^{-2(h+g)L}+\mathrm{e}^{-4hL}}$	hL
	$\mathrm{XT}_{\mathrm{diag}}$	$\dfrac{1-2\mathrm{e}^{-2(h+g)L}+\mathrm{e}^{-4hL}}{1+2\mathrm{e}^{-2(h+g)L}+\mathrm{e}^{-4hL}}$	$gL+h^2L^2$
$g=0$	$\mathrm{XT}_{\mathrm{adj}}$	$\tanh(hL)$	hL
	$\mathrm{XT}_{\mathrm{diag}}$	$\tanh^2(hL)$	h^2L^2

where $P_i(z)$ is the optical power in core i ($i = 1, 2, 3, 4$) and z represents the propagation direction. h and g are the average power-coupling coefficients (PCCs) [22, 23] between adjacent cores and between diagonal cores, respectively, and are assumed to be invariant along the z-axis.

The exact solutions of Eqs. (1a)–(1d) with and without g have been derived by Liang *et al.* [25] and Nakagawa *et al.* [24], respectively. In Refs. [24, 25], only the results are presented; thus, we show the procedure for deriving the exact solutions in Appendix.

When core i is excited with incident power P_{in}, $P_i(z = 0) = P_{\mathrm{in}}$, the exact solutions [24, 25] satisfy the power conservation relation as

$$P_i(z) + \sum_{j \neq i} P_j(z) = P_{\mathrm{in}}. \tag{2}$$

When $z = \infty$, the power is uniformly distributed as $P_1 = P_2 = P_3 = P_4 = P_{\mathrm{in}}/4$. The intercore XT from core i to core j ($j \neq i$) at $z = L$ is defined as

$$\mathrm{XT}_{ji} = \frac{P_j(L)}{P_i(L)}, \tag{3}$$

where L is the fiber length. Analytical expressions for intercore XT in square-layout UC-4CFs that are deduced from the exact solutions of Eqs. (1a)–(1d) [24, 25] are shown in Table I.

Although exact solutions of coupled-power equations are indispensable to the highly accurate evaluation of intercore XT in MCFs, it would be difficult to give a physical interpretation of intercore XT behavior. Thus, to make it easy to understand the physical mechanism of intercore XT behavior in square-layout UC-4CFs, we attempt to derive an approximate solution of Eqs. (1a)–(1d) that is valid for small XT values.

When core 1 is excited with incident power P_{in}, $P_1(z = 0) = P_{\mathrm{in}}$, on the basis of Ref. [10] in which a three-core model is introduced, we make the following assumptions:

$$P_1(z) \gg P_2(z) \gg P_3(z), \tag{4a}$$

$$P_1(z) \gg P_4(z) \gg P_3(z), \tag{4b}$$

$$g \ll h \ll 1, \tag{4c}$$

where we note that an average PCC exponentially decreases with increasing core-to-core distance [10] and that in square-layout UC-4CFs, the distance between diagonal cores is $\sqrt{2}$ times that between adjacent cores; therefore, g is sufficiently smaller than h. Considering the assumptions in Eqs. (4a)–(4c), Eqs. (1a)–(1d) are reduced to

$$P_1(z) \approx P_{\mathrm{in}}, \tag{5a}$$

$$\frac{\mathrm{d}P_2(z)}{\mathrm{d}z} = \frac{\mathrm{d}P_4(z)}{\mathrm{d}z} \approx hP_1(z), \tag{5b}$$

$$\frac{\mathrm{d}P_3(z)}{\mathrm{d}z} \approx gP_1(z) + hP_2(z) + hP_4(z), \tag{5c}$$

where owing to the very small XT, we also assume that the optical power in core 1 is not depleted.

Substituting Eq. (5a) into Eq. (5b) and noting $P_2(0) = P_4(0) = 0$, we obtain $P_2(z)$ and $P_4(z)$ as

$$P_2(z) = P_4(z) \approx hzP_{\mathrm{in}}. \tag{6}$$

Similarly, substituting Eqs. (5a) and (6) into Eq. (5c) and noting $P_3(0) = 0$, we obtain $P_3(z)$ as

$$P_3(z) \approx \left(gz + h^2z^2\right) P_{\mathrm{in}}. \tag{7}$$

From Eqs. (6) and (7), we have the approximate XT describing the fiber length dependence of adjacent XT ($\mathrm{XT}_{21} = \mathrm{XT}_{41} \equiv \mathrm{XT}_{\mathrm{adj}}$) and diagonal XT ($\mathrm{XT}_{31} \equiv \mathrm{XT}_{\mathrm{diag}}$), as shown in Table I. As is well known, $\mathrm{XT}_{\mathrm{adj}}$ is given by the product of h and L [22]. On the other hand, $\mathrm{XT}_{\mathrm{diag}}$ is given by the sum of $\mathrm{XT}_{\mathrm{dir}} = gL$ and $\mathrm{XT}_{\mathrm{indir}} = h^2L^2$. In the three-core model, $\mathrm{XT}_{\mathrm{indir}} = h^2L^2/2$ [10]. This is due to the fact that $\mathrm{XT}_{\mathrm{indir}}$ occurs via one neighboring core in the three-core model and via two neighboring cores in the present square-layout four-core model.

From Table I, we can see that $\mathrm{XT}_{\mathrm{adj}}$ grows linearly with increasing fiber length. However, this is not the case in $\mathrm{XT}_{\mathrm{diag}}$. $\mathrm{XT}_{\mathrm{diag}}$ has a specific fiber length at which $\mathrm{XT}_{\mathrm{dir}}$ and $\mathrm{XT}_{\mathrm{indir}}$ are equal to each other and this length is expressed as $L_{\mathrm{ip}} = g/h^2$ (intersecting point of $\mathrm{XT}_{\mathrm{dir}}$ and $\mathrm{XT}_{\mathrm{indir}}$ lines). $\mathrm{XT}_{\mathrm{diag}}$ is predominantly induced by $\mathrm{XT}_{\mathrm{dir}}$ under $L < L_{\mathrm{ip}}$ and by $\mathrm{XT}_{\mathrm{indir}}$ under $L > L_{\mathrm{ip}}$. That is, L_{ip} gives us a lower bound of fiber length beyond which $\mathrm{XT}_{\mathrm{diag}}$ grows quadratically. Note that such behavior in $\mathrm{XT}_{\mathrm{adj}}$ and $\mathrm{XT}_{\mathrm{diag}}$ does not last indefinitely. The reason is that as the fiber length increases, the accuracy of the approximate solution decreases.

Thus, using exact solutions, we define an application range of the approximate solution as follows:

$$\left|\mathrm{XT}_{\mathrm{approx}} - \mathrm{XT}_{\mathrm{exact}}\right| \leq 0.1\,\mathrm{dB}, \tag{8}$$

where $\mathrm{XT}_{\mathrm{approx}}$ is the approximate XT and $\mathrm{XT}_{\mathrm{exact}}$ is the exact XT.

Using the exact and approximate XTs in Table I and noting that when $\mathrm{XT}_{\mathrm{indir}}$ is predominant ($\mathrm{XT}_{\mathrm{diag}} \approx \mathrm{XT}_{\mathrm{indir}}$), $\mathrm{XT}_{\mathrm{dir}}$ is negligibly small (we can use the approximation $g \approx 0$), we obtain the maximum values of fiber length satisfying Eq. (8), namely, L_{adj} for $\mathrm{XT}_{\mathrm{adj}}$ and L_{diag} for $\mathrm{XT}_{\mathrm{diag}}$, by solving

$$\frac{hL_{\mathrm{adj}}}{\tanh\left(hL_{\mathrm{adj}}\right)} = 10^{0.01}, \tag{9a}$$

$$\frac{hL_{\mathrm{diag}}}{\tanh\left(hL_{\mathrm{diag}}\right)} = 10^{0.005}, \tag{9b}$$

where we note that in this case, the approximate XT is always greater than the exact XT.

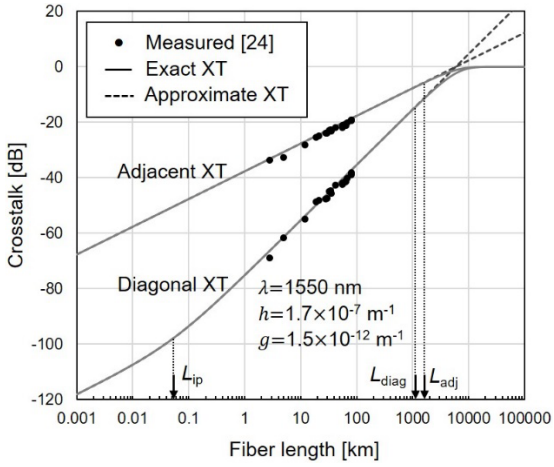

(a)

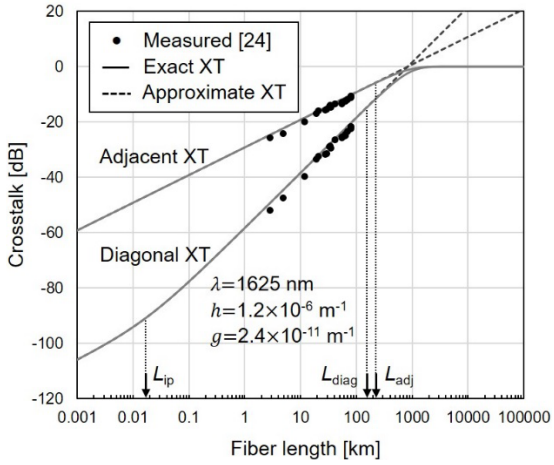

(b)

Fig. 2 Fiber length dependence of intercore crosstalk in the square-layout UC-4CF with homogeneous cores at the wavelength (λ) of (a) 1550 nm and (b) 1625 nm.

From Eqs. (9a) and (9b), we obtain $L_{\mathrm{adj}} \approx 0.265/h$ and $L_{\mathrm{diag}} \approx 0.187/h$. As a result, we can say that $\mathrm{XT}_{\mathrm{adj}}$ grows linearly under $L < L_{\mathrm{adj}}$ and that $\mathrm{XT}_{\mathrm{diag}}$ grows linearly under $L < L_{\mathrm{ip}}$ and quadratically under $L_{\mathrm{ip}} < L < L_{\mathrm{diag}}$.

3. Results and discussion

Here, we consider the square-layout UC-4CF shown in Fig. 1(b) [24]. The average distance between adjacent cores is 39.7 μm and that between diagonal cores is 56.1 μm [24]. The bending radius is assumed to be 155 mm. Using Eq. (25) in Ref. [22], the values of h and g are evaluated to be $1.7 \times 10^{-7}\,\mathrm{m}^{-1}$ and $1.5 \times 10^{-12}\,\mathrm{m}^{-1}$ at 1550 nm (C-band), respectively, and $1.2 \times 10^{-6}\,\mathrm{m}^{-1}$ and $2.4 \times 10^{-11}\,\mathrm{m}^{-1}$ at 1625 nm (L-band), respectively. Since the average PCCs (h and g) involve the mode-coupling coefficient [22, 23] which is expressed in terms of the overlap integral of electromagnetic fields [26], the overlap integral was numerically calculated.

Figs. 2(a) and (b) show the fiber length dependence of intercore XT values at 1550 nm and 1625 nm, respectively, where $g \neq 0$. Table II shows the values of L_{ip}, L_{diag}, and L_{adj}. From Figs. 2(a) and (b), we can see that the calculated

Table II L_{ip}, L_{diag}, and L_{adj}.

Wavelength	L_{ip}	L_{diag}	L_{adj}
1550 nm	~52 m	~1100 km	~1560 km
1625 nm	~17 m	~160 km	~220 km

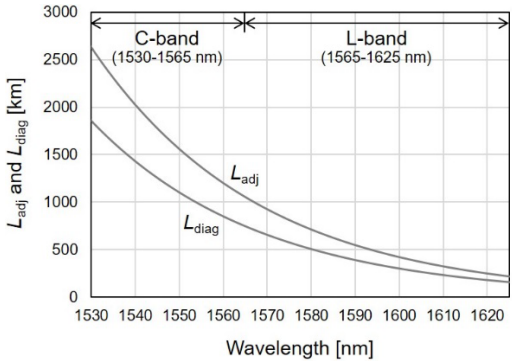

Fig. 3 Wavelength dependence of L_{adj} and L_{diag}.

results obtained using the exact-XT expression (solid lines) and approximate-XT expression (dashed lines) agree well with the measured results [24] denoted by dots. Note that the accuracy of the approximate solution decreases under $L > L_{\mathrm{adj}}$ and $L > L_{\mathrm{diag}}$.

In Ref. [24], the intercore XT was measured for fiber lengths ranging from 3 km to 80 km. Since the fiber length satisfies the conditions $L < L_{\mathrm{diag}}$ and $L < L_{\mathrm{adj}}$, the intercore XT behavior can be physically explained with the approximate-XT expression derived here. $\mathrm{XT}_{\mathrm{diag}}$ measurement in Ref. [24] was performed under $L_{\mathrm{ip}} < L < L_{\mathrm{diag}}$ within which $\mathrm{XT}_{\mathrm{indir}}$ is predominant; therefore, it follows that $\mathrm{XT}_{\mathrm{diag}}$ grows quadratically with fiber length [24]. Note that $\mathrm{XT}_{\mathrm{diag}}$ does not grow quadratically under $L < L_{\mathrm{ip}}$ and $L > L_{\mathrm{diag}}$, and that $\mathrm{XT}_{\mathrm{adj}}$ does not grow linearly under $L > L_{\mathrm{adj}}$.

Fig. 3 shows the wavelength dependence of L_{adj} and L_{diag} in the C-band (1530–1565 nm) and L-band (1565–1625 nm). L_{adj} and L_{diag} decrease exponentially with increasing wavelength.

4. Proposal of heterogeneous square-layout UC-4CFs

Thus far, we have discussed square-layout UC-4CFs with homogeneous cores. To further suppress not only $\mathrm{XT}_{\mathrm{diag}}$ but also $\mathrm{XT}_{\mathrm{bs}}$ and $\mathrm{XT}_{\mathrm{refl}}$, we propose the square-layout UC-4CF with heterogeneous cores shown in Fig. 4, where cores 2 and 4 are different from cores 1 and 3. In heterogeneous MCFs [27], not only identical cores but also non-identical cores are arranged so that the intercore XT between any pair of adjacent cores becomes sufficiently small; therefore, cores are more closely packed in a definite space than in a conventional, homogeneous MCF. Furthermore, the close packing of cores helps increase the outer cladding thickness (the minimum distance between the outermost core center and the cladding-coating interface), resulting in the suppression of coating-leakage loss (tunneling loss from the core to the fiber coating). Also, the XT relaxation can be used for the design of larger effective area which mitigates nonlinear

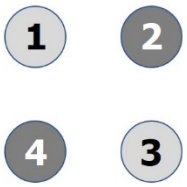

Fig. 4 Schematic of a square-layout UC-4CF with heterogenous cores.

effects in optical fibers and tighter core pitch which is advantageous to improve the rotation misalignment tolerance at the connection point [15].

For the heterogeneous UC-4CF shown in Fig. 4, coupled-power equations are given by

$$\frac{\mathrm{d}P_1(z)}{\mathrm{d}z} = \tilde{h}\,(P_2 - P_1) + g_1\,(P_3 - P_1) + \tilde{h}\,(P_4 - P_1), \quad (10a)$$

$$\frac{\mathrm{d}P_2(z)}{\mathrm{d}z} = \tilde{h}\,(P_1 - P_2) + \tilde{h}\,(P_3 - P_2) + g_2\,(P_4 - P_2), \quad (10b)$$

$$\frac{\mathrm{d}P_3(z)}{\mathrm{d}z} = g_1\,(P_1 - P_3) + \tilde{h}\,(P_2 - P_3) + \tilde{h}\,(P_4 - P_3), \quad (10c)$$

$$\frac{\mathrm{d}P_4(z)}{\mathrm{d}z} = \tilde{h}\,(P_1 - P_4) + g_2\,(P_2 - P_4) + \tilde{h}\,(P_3 - P_4), \quad (10d)$$

where $\tilde{h}$ is the average PCC between adjacent non-identical cores, and g_1 and g_2 are the average PCCs between identical cores 1 and 3 and between identical cores 2 and 4, respectively.

Analytical expressions for the intercore XT in square-layout UC-4CFs with heterogeneous cores are similar to those in Table I. When core 1 or 3 is excited at the fiber input end, h and g are replaced by $\tilde{h}$ and g_1, respectively. When core 2 or 4 is excited at the fiber input end, on the other hand, h and g are replaced by $\tilde{h}$ and g_2, respectively. When the distance between adjacent cores of the heterogeneous UC-4CF is the same as that of the homogeneous one, the relation $\tilde{h} < h$ holds in the non-phase matching region where the bending radius is larger than the so-called critical (or threshold) bending radius [21, 22, 23, 28, 29]; thus, in the heterogeneous UC-4CFs, not only $\mathrm{XT}_{\mathrm{diag}}$ but also $\mathrm{XT}_{\mathrm{bs}}$ and $\mathrm{XT}_{\mathrm{refl}}$ could be further suppressed ($\mathrm{XT}_{\mathrm{bs}}$ and $\mathrm{XT}_{\mathrm{refl}}$ are proportional to the average PCC between adjacent cores [15]).

When $\tilde{h} \approx g_l$ ($l = 1, 2$) or $\tilde{h} < g_l$, we note that the assumptions in Eqs. (4a)–(4c) made in deriving Eqs. (5a)–(5c) do not hold and that it is necessary to rewrite the analytical expressions for the intercore XT in homogeneous UC-4CFs shown in Table I.

As an example, when $\tilde{h} \approx g_l$, from Table I we obtain the exact XT as

$$\mathrm{XT}_{\mathrm{adj}} = \mathrm{XT}_{\mathrm{diag}} = \frac{1 - \mathrm{e}^{-4\tilde{h}L}}{1 + 3\mathrm{e}^{-4\tilde{h}L}}, \quad (11)$$

and the approximate XT as

$$\mathrm{XT}_{\mathrm{adj}} = \mathrm{XT}_{\mathrm{diag}} = \tilde{h}L. \quad (12)$$

The maximum fiber length satisfying Eq. (8), L_{adj} for $\mathrm{XT}_{\mathrm{adj}}$, is obtained by solving

$$\frac{\tilde{h}L_{\mathrm{adj}}\left(1 + 3\mathrm{e}^{-4\tilde{h}L_{\mathrm{adj}}}\right)}{1 - \mathrm{e}^{-4\tilde{h}L_{\mathrm{adj}}}} = 10^{-0.01}, \quad (13)$$

where we note that in the small XT region, the approximate XT is less than the exact XT. Obviously, L_{diag} for $\mathrm{XT}_{\mathrm{diag}}$ is equal to L_{adj}. From Eq. (13), we have $L_{\mathrm{adj}} = L_{\mathrm{diag}} \approx 0.0235/\tilde{h}$. As a result, we can say that both $\mathrm{XT}_{\mathrm{adj}}$ and $\mathrm{XT}_{\mathrm{diag}}$ grow linearly under $L < L_{\mathrm{adj}} = L_{\mathrm{diag}}$. In this case, i.e., $\tilde{h} \approx g_l \ll h$, the lengths denoted by L_{adj} and L_{diag} in the heterogeneous UC-4CF become markedly higher than those in the homogeneous one.

5. Conclusion

The behavior of intercore XT in square-layout UC-4CFs was investigated on the basis of a coupled-power theory. To make it easy to understand the physical mechanism of intercore XT behavior, we derived an approximate solution of coupled-power equations. We showed that there exists a range of fiber lengths within which $\mathrm{XT}_{\mathrm{diag}}$ grows quadratically. Finally, we proposed a heterogeneous square-layout UC-4CF and suggested that not only $\mathrm{XT}_{\mathrm{diag}}$ but also $\mathrm{XT}_{\mathrm{bs}}$ and $\mathrm{XT}_{\mathrm{refl}}$ could be further suppressed.

A square-layout UC-4CF with standard 125-μm cladding is also suitable for O-band (1260–1360 nm) short-reach transmission. Other types of 125-μm-cladding short-reach UC-4CFs of which cores are arranged in a trapezoidal layout [15] or a linear array [15, 30] have also been fabricated. The theoretical model described here can be extended to such non-square-layout UC-4CFs.

References

[1] Y. Tamura, *et al.*: "Low-loss uncoupled two-core fiber for power efficient practical submarine transmission," Proc. OFC (2019) M1E.5 (DOI: 10.1364/OFC.2019.M1E.5).
[2] T. Matsui, *et al.*: "Design of 125 μm cladding multi-core fiber with full-band compatibility to conventional single-mode fiber," Proc. ECOC (2015) We.1.4.5 (DOI: 10.1109/ECOC.2015.7341966).
[3] H. Sakuma, *et al.*: "125-μm-cladding low-loss uncoupled four-core fiber," Proc. EXAT (2019) P-13 (DOI: 10.34385/proc.31.P-13).
[4] Y. Sagae, *et al.*: "Ultra-low-XT multi-core fiber with standard 125-μm cladding for long-haul transmission," Proc. OECC (2019) TuC3-4 (DOI: 10.23919/PS.2019.8817672).
[5] T. Matsui, *et al.*: "Step-index profile multi-core fibre with standard 125 μm cladding to full-band application," Proc. ECOC (2019) M.1.D.3 (DOI: 10.1049/cp.2019.0751).
[6] M. Takahashi, *et al.*: "Uncoupled 4-core fibre with ultra-low loss and low inter core crosstalk," Proc. ECOC (2020) Th1A-5 (DOI: 10.1109/ECOC48923.2020.9333161).
[7] T. Gonda, *et al.*: "125 μm 5-core fibre with heterogeneous design suitable for migration from single-core system to multi-core system," Proc. ECOC (2016) W.2.B.1.
[8] T. Gonda, *et al.*: "Design of multicore fiber having upgradability from standard single-mode fibers and its application," J. Lightw. Technol. **37** (2019) 396 (DOI: 10.1109/JLT.2019.2895903).
[9] T. Hayashi, *et al.*: "125-μm-cladding 8-core multi-core fiber realizing ultra-high-density cable suitable for O-band short-reach optical interconnects," Proc. OFC (2015) Th5C.6 (DOI: 10.1364/OFC.2015.Th5C.6).
[10] T. Hayashi, *et al.*: "125-μm-cladding eight-core multi-core fiber realizing ultra-high-density cable suitable for O-band short-reach optical interconnects," J. Lightw. Technol. **34** (2016) 85 (DOI: 10.1109/JLT.2015.2470078).
[11] T. Matsui, *et al.*: "118.5 Tbit/s transmission over 316 km-long multi-core fiber with standard cladding diameter," Proc. OECC (2017) PDP2 (DOI: 10.1109/OECC.2017.8115049).
[12] B.J. Puttnam, *et al.*: "319 Tb/s transmission over 3001 km with S, C and L band signals over > 120 nm bandwidth in 125 μm wide 4-core

fiber," Proc. OFC (2021) F3B.3 (DOI: 10.1364/OFC.2021.F3B.3).
[13] D. Soma, *et al.*: "Trans-Pacific class transmission over a standard cladding ultralow-loss 4-core fiber," Opt. Express **30** (2022) 9482 (DOI: 10.1364/OE.453597).
[14] B.J. Puttnam, *et al.*: "1 Pb/s transmission in a 125 μm diameter 4-core MCF," Proc. CLEO (2022) JTh6B.1.
[15] T. Hayashi, *et al.*: "Uncoupled multi-core fiber design for practical bidirectional optical communications," Proc. OFC (2022) M1E.1 (DOI: 10.1364/OFC.2022.M1E.1).
[16] T. Ito, *et al.*: "Reduction of influence of inter-core cross-talk in MCF with bidirectional assignment between neighboring cores," Proc. OFC (2013) OTh3K.2 (DOI: 10.1364/OFC.2013.Oth3K.2).
[17] A. Sano, *et al.*: "Crosstalk-managed high capacity long haul multicore fiber transmission with propagation-direction interleaving," J. Lightw. Technol. **32** (2014) 2771 (DOI: 10.1109/JLT.2014.2320826).
[18] F. Ye, *et al.*: "High-count multi-core fibers for space-division multiplexing with propagation-direction interleaving," Proc. OFC (2015) Th4C.3 (DOI: 10.1364/OFC.2015.Th4C.3).
[19] M. Arikawa, *et al.*: "Crosstalk reduction with bidirectional signal assignment on square lattice structure 16-core fiber over WDM transmission for gradual upgrade of SMF-based lines," J. Lightw. Technol. **34** (2016) 1908 (DOI: 10.1109/JLT.2015.2509472).
[20] K. Takenaga, *et al.*: "An investigation on crosstalk in multi-core fibers by introducing random fluctuation along longitudinal direction," IEICE Trans. Commun. **E94-B** (2011) 409 (DOI: 10.1587/transcom.E94.B.409).
[21] M. Koshiba, *et al.*: "Multi-core fiber design and analysis: coupled-mode theory and coupled-power theory," Opt. Express **19** (2011) B102 (DOI: 10.1364/OE.19.00B102).
[22] M. Koshiba, *et al.*: "Analytical expression of average power-coupling coefficients for estimating intercore crosstalk in multicore fibers," IEEE Photon. J. **4** (2012) 1987 (DOI: 10.1109/JPHOT.2012.2221085).
[23] T. Hayashi, *et al.*: "Physical interpretation of intercore crosstalk in multicore fiber: effects of macrobend, structure fluctuation, and microbend," Opt. Express **21** (2013) 5401 (DOI: 10.1364/OE.21.005401).
[24] M. Nakagawa, *et al.*: "Estimating crosstalk between diagonal cores in four-core fibers with square lattice structure," Proc. OECC (2022) TuC2-3 (DOI: 10.23919/oecc/psc53152.2022.9850117).
[25] Y. Liang, *et al.*: "Theoretical study of four-core five-mode microstructured fiber with low crosstalk and large mode field area," Chin. J. Lasers **48** (2021) 1906004 (DOI: 10.3788/CJL202148.1906004).
[26] K. Okamoto: *Fundamentals of Optical Waveguides* (Academic Press, Cambridge, MA, USA, 2021) 3rd ed. (DOI: 10.1016/C2017-0-02432-1).
[27] M. Koshiba, *et al.*: "Heterogeneous multi-core fibers: proposal and design principle," IEICE Electron. Express **6** (2009) 98 (DOI: 10.1587/elex.6.98).
[28] K. Saitoh, *et al.*: "Low-crosstalk multi-core fibers for long-haul transmission," Proc. SPIE **8284** (2012) 82840I (DOI: 10.1117/12.909473).
[29] Y. Amma, *et al.*: "High-density multicore fiber with heterogeneous core arrangement," Proc. OFC (2015) Th4C.4 (DOI: 10.1364/OFC.2015.Th4C.4).
[30] X. Chen, *et al.*: "Demonstration of 1 Tb/s transmission over 6.3-km 1×4 linear array multicore fiber with standard 125-μm cladding," Opt. Fiber Technol. **71** (2022) 102941 (DOI: 10.1016/j.yofte.2022.102941).

Appendix

Eqs. (1a)–(1d) are a set of simultaneous ordinary differential equations. These equations can be converted into a matrix form and the coefficient matrix has three eigenvalues: 0, $-2(h+g)$, and $-4h$. The eigenvalue $-2(h+g)$ is doubly degenerate. In general, it is complicated to obtain the eigenvectors corresponding to the degenerate eigenvalue.

Here, to resolve the degeneracy problem, we note that when core 1 is excited at the fiber input end ($z = 0$), $P_2(z)$ and $P_4(z)$ are equal to each other, and we define P_{24} as $P_{24}(z) \equiv P_2(z) + P_4(z)$ and rewrite Eqs. (1a)–(1d) as

$$\frac{\mathrm{d}P_1(z)}{\mathrm{d}z} = -(2h+g)P_1 + hP_{24} + gP_3, \tag{14a}$$

$$\frac{\mathrm{d}P_{24}(z)}{\mathrm{d}z} = 2hP_1 - 2hP_{24} + 2hP_3, \tag{14b}$$

$$\frac{\mathrm{d}P_3(z)}{\mathrm{d}z} = gP_1 + hP_{24} - (2h+g)P_3. \tag{14c}$$

A general solution of Eqs. (14a)–(14c) is given by

$$\begin{bmatrix} P_1(z) \\ P_{24}(z) \\ P_3(z) \end{bmatrix} = \sum_{k=1}^{3} C_k \mathrm{e}^{\gamma_k z} \boldsymbol{V}_k, \tag{15}$$

where C_k ($k = 1,2,3$) is the arbitrary constant, and γ_k and $\boldsymbol{V}_k$ are the eigenvalue and eigenvector of Eqs. (14a)–(14c), respectively, as shown in Table III. For simplicity, the eigenvectors are not normalized (it is not always necessary to normalize the eigenvectors).

Applying the initial conditions $P_1(0) = P_{\mathrm{in}}$ and $P_{24}(0) = P_3(0) = 0$ to Eq. (15), and using $\boldsymbol{V}_k$, we determined the arbitrary constants as

$$C_1 = C_2/2 = C_3 = P_{\mathrm{in}}/4. \tag{16}$$

Then, using γ_k, $\boldsymbol{V}_k$, and C_k, and noting $P_2(z) = P_4(z) = P_{24}(z)/2$, from Eq. (15) we have the exact solutions derived by Liang *et al.* ($g \neq 0$) [25] and Nakagawa *et al.* ($g = 0$) [24]. When core 3 is excited at the fiber input end, we note that the initial conditions are given by $P_3(0) = P_{\mathrm{in}}$ and $P_1(0) = P_{24}(0) = 0$. When core 2 or 4 is excited at the fiber input end, we note that $P_1(z) = P_3(z)$ and set $P_1(z) + P_3(z)$ to $P_{13}(z)$ in place of $P_{24}(z)$.

Table IV shows the eigenvalues and eigenvectors of Eqs. (10a)–(10d) for heterogeneous square-layout UC-4CFs. Eqs. (10a)–(10d) have four eigenvalues, all of which are not degenerate.

Table III Eigenvalues and eigenvectors of Eqs. (14a)–(14c).

k	1	2	3
γ_k	0	$-2(h+g)$	$-4h$
$\boldsymbol{V}_k$	$\begin{bmatrix}1\\2\\1\end{bmatrix}$	$\begin{bmatrix}1\\0\\-1\end{bmatrix}$	$\begin{bmatrix}1\\-2\\1\end{bmatrix}$

Table IV Eigenvalues and eigenvectors of Eqs. (10a)–(10d).

k	1	2	3	4
γ_k	0	$-2(\tilde{h}+g_1)$	$-2(\tilde{h}+g_2)$	$-4\tilde{h}$
$\boldsymbol{V}_k$	$\begin{bmatrix}1\\1\\1\\1\end{bmatrix}$	$\begin{bmatrix}1\\0\\-1\\0\end{bmatrix}$	$\begin{bmatrix}0\\1\\0\\-1\end{bmatrix}$	$\begin{bmatrix}1\\-1\\1\\-1\end{bmatrix}$